Chapter 10
Non-traditional Stable Isotope Geochemistry of Seep Deposits

Meng Jin and Dong Feng

Abstract Non-traditional stable isotope geochemistry is a useful tool for revealing element migration, transformation and circulation in geological processes. A series of biogeochemical processes result in special and variable sedimentary environments in seep systems. Many elements are impacted and involved in different biogeochemical processes in seep systems, especially the formation of authigenic minerals, making seep deposits archives for studying elemental and isotopic behaviors in natural environments. Iron (Fe) and molybdenum (Mo) are involved in the formation of pyrite, and magnesium (Mg) and calcium (Ca) are closely related to the precipitation of authigenic carbonate. Research on the Fe, Mo, Mg and Ca isotopic compositions of different seep deposits from the South China Sea has been conducted in recent years. Preliminary studies have provided new insights into the mechanisms of isotopic fractionation and element cycling during early diagenesis. In this chapter, we provide an overview of the current understanding of the Fe, Mo, Mg and Ca isotope geochemistry of seep deposits from the South China Sea, targeting authigenic minerals, sediments and pore fluids.

10.1 Introduction

Traditional stable isotope geochemistry usually refers to isotopes of C, H, O, N and S. With the development of multicollector inductively coupled plasma–mass spectrometry (MC–ICP–MS), high-precision measurements of more isotopes have led to the thriving of so-called non-traditional stable isotope geochemistry (Halliday

M. Jin (✉)
MNR Key Laboratory of Marine Mineral Resources, Guangzhou Marine Geological Survey, Guangzhou 511458, China
e-mail: jinmeng17@mails.ucas.ac.cn

National Engineering Research Center for Gas Hydrate Exploration and Development, Guangzhou 511458, China

D. Feng
College of Marine Sciences, Shanghai Ocean University, Shanghai 201306, China
e-mail: dfeng@shou.edu.cn

D. Chen and D. Feng (eds.), *South China Sea Seeps*,
https://doi.org/10.1007/978-981-99-1494-4_10

et al. 1995). The distinctive geochemical features of these non-traditional stable isotopes, such as diverse geochemical activity, various concentrations in different geological reservoirs, redox sensitivity, and the links to biological activities, make them unique tracers for different geological processes (Teng et al. 2017).

The formation of authigenic minerals at seeps involves element migration and corresponding isotope fractionation, such as Fe and Mo for pyrite and Mg and Ca for carbonate. In addition, the geochemical processes in the cold seep system leads to changes in the redox state in the environment and involves the isotope fractionation of redox-sensitive elements, such as Mo. The seep system is an excellent "laboratory" for studying the behaviors of these isotopes in the natural environment. These isotopic compositions of different seep deposits have been successively analyzed in recent years. The South China Sea is one of the most investigated seep systems, and various non-traditional stable isotope geochemical techniques have been used to explore various geochemical processes. Iron isotopic compositions of anaerobic oxidation of methane (AOM)-derived pyrite from several sites provide constraints on the relationship with AOM activity and pyrite formation (Lin et al. 2017, 2022). The Mo enrichment and isotopic composition of sediments and carbonates provide new insights into the geochemical cycling of Mo (Lin et al. 2021). Magnesium isotopic compositions of pore water from "Haima" and seep carbonate from the Dongsha area put forward a new understanding of the behavior of Mg isotopes during carbonate precipitation (Jin et al. 2021, 2022). Studies of the Ca isotope geochemistry of dolomite from the Dongsha area have constrained the process of carbonate formation (Wang et al. 2012, 2013).

10.2 Fe Isotopes

Iron is a major widely distributed element in the silicate Earth. It has three oxidation states, namely, metallic iron, ferrous iron and ferric iron, which lead to its complex chemical and isotopic behaviors. Iron has four stable isotopes, with mass numbers of 54, 56, 57 and 58, which represent 5.845%, 91.754%, 2.119%, and 0.282% of the total mass, respectively (Meija et al. 2016). The Fe isotope ratios are usually reported as δ^{56}Fe:

$$\delta^{56}\mathrm{Fe} = \left[\frac{\left(^{56}\mathrm{Fe}/^{54}\mathrm{Fe}\right)_{\mathrm{sample}}}{\left(^{56}\mathrm{Fe}/^{54}\mathrm{Fe}\right)_{\mathrm{standard}}} - 1 \right] \times 1000$$

where the standard usually refers to IRMM-14. Another standard, the average of terrestrial igneous rocks (IgRx), was previously used to define the isotopic composition of Fe (Beard and Johnson 1999). The conversion of δ^{56}Fe values relative to the two standards can be adjusted according to Beard et al. (2003a):

$$\delta^{56}\mathrm{Fe}_{\mathrm{IRMM-14}} = \delta^{56}\mathrm{Fe}_{\mathrm{IgRx}} + 0.09‰$$

in the following text, $\delta^{56}Fe$ values refer to $\delta^{56}Fe_{IRMM\text{-}14}$ unless noted otherwise.

Pyrite is a common mineral in anoxic marine sediments, and its sulfur isotopic composition serves as an archive for constraining the biochemical cycle of sulfur and the evolution of ocean chemistry (Canfield and Teske 1996; Farquhar et al. 2000; Bekker et al. 2004; Johnston et al. 2006; Pasquier et al. 2017). The geochemical cycles of sulfur and iron are intimately coupled and recorded in sedimentary pyrite (Rouxel et al. 2005; Johnson et al. 2008; Hofmann et al. 2009; Liu et al. 2020). Pyrite in seep systems can present as framboids, overgrowths and euhedral crystals in sediments or enclosed in seep carbonates (e.g., Peckmann et al. 2001; Lin et al. 2016). The variable sulfur isotopic compositions of pyrite are closely related to AOM activity (e.g., Jørgensen et al. 2004; Borowski et al. 2013). The study of Fe isotope geochemistry may be useful to better understand the formation process of pyrite in seep systems. The Fe isotopic composition of pyrite depends on (1) the Fe isotopic composition of Fe sources and (2) the fractionation of Fe isotopes during the formation of pyrite (Butler et al. 2005; Guilbaud et al. 2011; Dauphas et al. 2017). Terrigenous active iron minerals are the main iron source for pyrite formation in continental margin sediments (Berner 1970; Poulton et al. 2004). Both theoretical calculations and experiments show that ferrous iron is ^{56}Fe-depleted compared to ferric iron that is either dissolved or contained in minerals (Johnson et al. 2002; Welch et al. 2003). Aqueous Fe^{2+} is released into pore water during dissimilatory iron reduction (DIR), with fractionation of $-0.5‰$ to $-2.95‰$ between aqueous Fe^{2+} and Fe oxides (Dauphas et al. 2017 and references therein). In addition, abiotic reductive dissolution by sulfide and iron-mediated anaerobic oxidation of methane (Fe-AOM) can also release isotopically lighter Fe into pore water (Riedinger et al. 2014; Egger et al. 2015). Hydrogen sulfide produced by organoclastic sulfate reduction and AOM reacts with dissolved iron or reactive iron minerals to form metastable intermediates, such as mackinawite, pyrrhotite and greigite, which are finally converted into pyrite (Jørgensen and Kasten 2006). The $\Delta^{56}Fe_{Fe(II)\text{-}FeS}$ are $-0.52 \pm 0.16‰$ in equilibrium at 2 °C and $+0.85 \pm 0.3‰$ in kinetic fractionation (Butler et al. 2005; Wu et al. 2012). The fractionation of Fe between FeS and pyrite is $+2.20 \pm 0.70‰$ (Guilbaud et al. 2011). Combining all these processes, potential fractionation between aqueous Fe^{2+} and pyrite can vary from $-3.1‰$ to $+0.5‰$ depending on different extents of pyritization (Guilbaud et al. 2011).

To date, the reported $\delta^{56}Fe$ values of bulk pyrite from seeps in the South China Sea range from $-1.48‰$ to $+0.38‰$ (n = 42) (Lin et al. 2017, 2018), similar to the range of variation in $\delta^{56}Fe$ values of other sedimentary pyrites (Fig. 10.1). The Fe isotopic compositions of bulk sediment at seeps from the South China Sea ($\delta^{56}Fe = +0.038‰$ to $+0.122‰$, n = 17; Fig. 10.1) are also close to those of other modern marine sediments ($\delta^{56}Fe = -0.12‰$ to $+0.23‰$; Beard et al. 2003b; Severmann et al. 2006; Fehr et al. 2010). However, in situ analyses of the Fe isotopic compositions of pyrite aggregates of different types from seeps by LA–MC–ICP–MS revealed large variations in $\delta^{56}Fe$ values ranging from $-1.09‰$ to $+1.90‰$ (n = 160) (Lin et al. 2018).

The iron pools in marine sediments include iron oxyhydroxides (Fe_{ox}), magnetite (Fe_{mag}), carbonate (Fe_{carb}), silicate (Fe_{sil}), and pyrite (Fe_{py}). Highly reactive iron

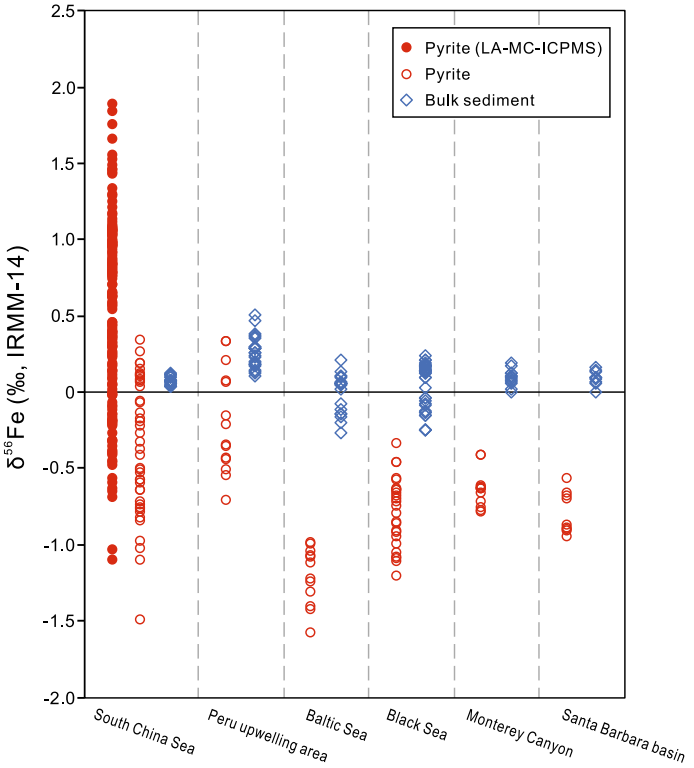

Fig. 10.1 Comparison of iron isotopic compositions of bulk sediment and pyrite from modern marine environments. Data from the South China Sea are from Lin et al. (2017, 2018). Data for the Peru upwelling area are from Scholz et al. (2014). Data from the Baltic Sea are from Fehr et al. (2008, 2010). Data from the Black Sea and Santa Barbara are from Severmann et al. (2006). Note that the pyrites from the South China Sea were hand-picked, while those from other studies were obtained through a chemical leaching procedure; see details in Severmann et al. (2006)

(Fe_{HR}) is defined as the sum of Fe_{ox}, Fe_{mag}, Fe_{carb} and Fe_{py}, and Fe_{py}/Fe_{HR} is introduced to indicate the extent of pyritization (e.g., Scholz et al. 2014; Lin et al. 2017, 2018). Researchers have suggested that iron oxyhydroxides and magnetite are the major iron sources for the precipitation of pyrite at seeps in the South China Sea (Lin et al. 2017, 2018). The enrichment of ^{56}Fe in pyrite is consistent with the increased degree of pyritization in the South China Sea (Fig. 10.2a). It has been suggested that $\delta^{56}Fe$ values of pyrite are controlled by both sulfide availability and iron pools in seep systems (Lin et al. 2018). A positive correlation between $\delta^{56}Fe$ and $\delta^{34}S$ values of pyrite has been observed, and pyrite affected by AOM and organoclastic sulfate reduction can be distinguished by different Fe and S isotopic compositions (Fig. 10.2b; Lin et al. 2017). In situ analysis of $\delta^{56}Fe$ indicates that the later-stage overgrowths and euhedral pyrites are more enriched in ^{56}Fe than the earlier formed

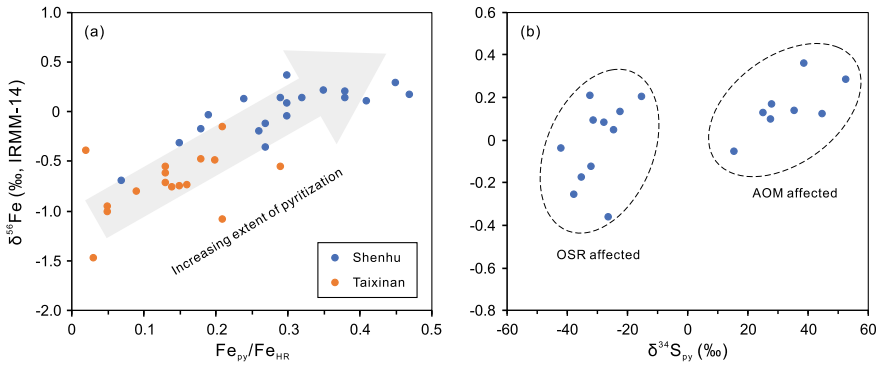

Fig. 10.2 Enrichment of ^{56}Fe in pyrite with increasing extent of pyritization (**a**) and plot of δ^{56}Fe against δ^{34}S of pyrite from the Shenhu area in the South China Sea (**b**). Modified after Lin et al. (2017, 2018)

framboids (Lin et al. 2018). This finding has been explained by Rayleigh-type distillation owing to the relatively Fe-limited environment within sediment during the formation of later-stage pyrite (Lin et al. 2022). The combination of Fe and S isotopic compositions of pyrite from seeps serves as a potential proxy to trace the different biogeochemical processes in early diagenesis.

10.3 Mo Isotopes

Molybdenum is a transition element with a wide range of redox states (–IV to +VIII), leading to its high degree of chemical reactivity. Molybdenum (IV) and Mo (VI) are most common on Earth's surface. Molybdenum has seven stable isotopes (mass numbers of 92, 94, 95, 96, 97, 98 and 100) with similar abundances of approximately 10% to 25% (Hlohowskyj et al. 2021). The isotopic composition of Mo is expressed as δ^{98}Mo relative to NIST-SRM-3134 = 0.25‰ (Nägler et al. 2014):

$$\delta^{98}\mathrm{Mo} = \left[\frac{\left(^{98}\mathrm{Mo}/^{95}\mathrm{Mo}\right)_{\mathrm{sample}}}{\left(^{98}\mathrm{Mo}/^{95}\mathrm{Mo}\right)_{\mathrm{NIST-SRM-3134}}} - 1 \right] \times 1000 + 0.25‰$$

where +0.25‰ accounts for the offset from the in-house standards used previously (Nägler et al. 2014).

Molybdenum has a long residence time of ~0.44 to 0.8 Ma and is generally ubiquitous (~105 nM) in oxygenated oceans (Miller et al. 2011; Nakagawa et al. 2012; Hlohowskyj et al. 2021). The Mo isotopic composition (~2.3‰) is also homogenous in modern open seawater (Hlohowskyj et al. 2021). Molybdenum is redox sensitive and has characteristic isotopic fractionation (Kendall et al. 2017). The Mo isotopic

signatures in sediments have been used as a proxy to reconstruct marine redox conditions (e.g., Poulson et al. 2006; Scott and Lyons 2012; Kendall et al. 2017 and references therein). In oxic environments, Mo mainly presents as molybdate (MoO_4^{2-}) in seawater (Siebert et al. 2003). The dissolved Mo can easily absorb to metal oxides, leading to $\Delta^{98}Mo_{seawater\text{-}solid}$ of approximately 0.8‰ to 3.2‰ (e.g., Barling et al. 2001; Siebert et al. 2003; Wasylenki et al. 2008; Scholz et al. 2017). Under anoxic/sulfidic conditions, MoO_4^{2-} transforms to thiomolybdates ($MoO_xS_{(4-x)}^{2-}$) facilitated by hydrogen sulfide, which is easily captured by iron sulfide or sulfur-rich organic matter and then stored in sediments (Helz et al. 1996, 2011; Tribovillard et al. 2006). The removal of Mo from aqueous environments is mainly controlled by the availability of dissolved hydrogen sulfide (Kendall et al. 2017). At $[H_2S]_{aq}$ > 11 μM, Mo is quantitatively transformed into tetrathiomolybdate and scavenges into sediments (Erickson and Helz 2000). The sediments record the Mo isotopic composition of ambient water (Nägler et al. 2011). Under conditions with $[H_2S]_{aq}$ < 11 μM, sediment yields a large variation in Mo isotopic composition due to incomplete sulfurization from molybdate to tetrathiomolybdate (Erickson and Helz 2000; Neubert et al. 2008; Nägler et al. 2011).

The AOM in seep systems create strongly sulfidic environmental conditions in pore water, with $[H_2S]_{aq}$ easily exceeding 11 μM in the case of high methane flux (e.g., Gieskes et al. 2005, 2011; Joye et al. 2010). This facilitates the accumulation of authigenic Mo in sediments or seep carbonates. The enrichment of Mo in seep sediment and the covariation of Mo and U in seep carbonate are strongly associated with redox states and the intensity of AOM (Hu et al. 2014; Chen et al. 2016). Seeps may serve as an important sink in the marine geochemical cycle of Mo (Hu et al. 2015). Therefore, Mo isotope geochemistry can provide new insights into tracing the sedimentary environment in seep systems. To date, only sparse data on the Mo isotopic composition of sediments and carbonates at seeps have been reported (Lin et al. 2021). The δ^{98}Mo values of bulk sediment and carbonate nodules from the South China Sea range from +0.2‰ to +2.0‰ (n = 36) and +1.4‰ to +2.1‰ (n = 5), respectively (Fig. 10.3; Lin et al. 2021). The large variation in Mo isotopic compositions of sediment was ascribed to the mixing of authigenic Mo sequestered in the course of AOM and detrital Mo in sediment unaffected by seepage. In addition, the later-formed pyrite may also cause additional Mo accumulation and influence the δ^{98}Mo of bulk sediment (Lin et al. 2021). For seep carbonate with a narrow range of δ^{98}Mo values, the offset between $\delta^{98}Mo_{carbonate}$ and $\delta^{98}Mo_{seawater}$ is close to that of strongly euxinic conditions (Lin et al. 2021). Considering the much higher H_2S concentration in active seepage than the critical Mo speciation threshold of ~11 μM, $\delta^{98}Mo_{carbonate}$ was thought to have potential for tracing the Mo isotopic composition of seawater (Lin et al. 2021).

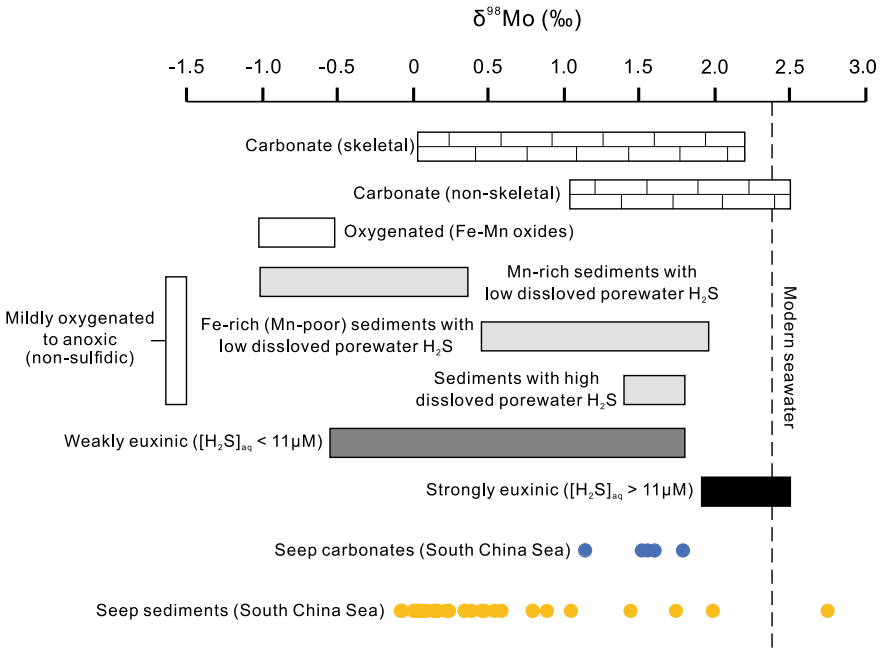

Fig. 10.3 Molybdenum isotopic compositions of seep carbonates and sediments from the South China Sea (Lin et al. 2021) and other sinks of Mo in the modern oceans (modified after Kendall et al. 2017)

10.4 Mg Isotopes

Magnesium is widely distributed in the silicate Earth, hydrosphere and biosphere. It has three stable isotopes, i.e., ^{24} Mg, ^{25} Mg and ^{26} Mg, with typical abundances of 78.97%, 10.01% and 11.03%, respectively (Meija et al. 2016). The isotopic composition of Mg is usually reported as δ^{26}Mg relative to the DSM3 standard (Young and Galy 2004):

$$\delta^{26}\mathrm{Mg} = \left[\frac{\left(^{26}\mathrm{Mg}/^{24}\mathrm{Mg}\right)_{\mathrm{sample}}}{\left(^{26}\mathrm{Mg}/^{24}\mathrm{Mg}\right)_{\mathrm{DSM3}}} - 1\right] \times 1000$$

Magnesium is the second most abundant cation in seawater, with a long residence time of ~13 Ma (Li 1982). The Mg isotopic composition of modern seawater is −0.83 ± 0.09‰ (Ling et al. 2011). Carbonate precipitation represents a sink of Mg in the ocean and is an important part of the oceanic Mg cycle (Higgins and Schrag 2015). The Mg isotopic composition of marine carbonates serves as a tool for unraveling the geochemical cycling of Mg in the ocean on geological timescales (e.g., Tipper et al. 2006; Higgins and Schrag 2012, 2015; Fantle and Higgins 2014). Carbonate is generally enriched in ^{24} Mg relative to seawater and displays a large variation in δ^{26}Mg

(Teng 2017). Fractionation of Mg isotopes during carbonate precipitation represents a temperature dependence of only approximately 0.01‰ $°C^{-1}$, while it exhibits a strong mineralogical control (Saenger and Wang 2014). The order of enrichment from light to heavy isotopes is calcite < magnesite < dolomite < aragonite (Saenger and Wang 2014). In addition, the Mg isotopic composition of carbonate could also be influenced by other factors, such as the precipitation rate, inorganic and organic ligands in solution, and biological effects (Saenger and Wang 2014 and references therein; Schott et al. 2016; Mavromatis et al. 2017).

Most seep carbonates from the South China Sea are composed of microcrystalline high-Mg calcite (HMC) and aragonite cement. In addition, a significant amount of microcrystalline dolomite occurs at some seep sites (Feng et al. 2018 and references therein). The content of $MgCO_3$ in some HMCs can even reach 38 mol%, occurring in association with minor amounts of dolomite (Han et al. 2008). Previous studies have confirmed that the presence of hydrogen sulfide provided by AOM can prominently affect the incorporation of Mg into carbonate minerals (e.g., Naehr et al. 2007; Zhang et al. 2012; Lu et al. 2018, 2021; Tong et al. 2019). Therefore, seep deposits are good subjects for understanding the behavior of Mg isotopes during carbonate precipitation in natural environments. The Mg^{2+} in seawater diffusing into pore water is the main source of Mg in seep carbonates. The $\delta^{26}Mg$ of pore water from an active seep in the South China Sea ranges from −0.88‰ to −0.71‰ (from 0 to 8 meter below the seafloor), similar to that of seawater (Jin et al. 2022). A slight increase in the pore water $\delta^{26}Mg$ values with depth indicates the precipitation of authigenic carbonate. This occurs because the sufficient replenishment of Mg from seawater is far greater than the consumption of Mg in pore water during precipitation of authigenic carbonate (Jin et al. 2022). Lu et al. (2017) and Jin et al. (2021) analyzed the Mg isotopic composition of seep carbonates from the South China Sea. A comparison of the $\delta^{26}Mg$ values of seep carbonates and other marine carbonates is presented in Fig. 10.4. The $\delta^{26}Mg$ values of seep carbonates display a smaller range of variation relative to those of other marine carbonates. Additionally, the biologically mediated vital effects on the Mg isotopic composition are not obvious compared to biodetrital carbonates based on current data. Carbonates in Lu et al. (2017) consist mainly of dolomite, with relatively consistent Mg isotopic compositions ($\delta^{26}Mg = -2.45‰$ to −2.15‰, n = 11). However, the $\delta^{26}Mg$ values of HMC in pipe-like seep carbonates vary from −3.42‰ to − 2.63‰ (n = 10), and a decreasing trend of $\delta^{26}Mg$ values from the periphery to the inner portion of the "pipe" was observed (Jin et al. 2021).

The correlation of inorganic $\delta^{13}C$ and $\delta^{26}Mg$ values of seep carbonates is considered to be related to the dissolved hydrogen sulfide in pore water produced by AOM (Lu et al. 2017; Jin et al. 2021). The existence of dissolved H_2S has been confirmed to promote the incorporation of Mg into carbonate in precipitation experiments (Zhang et al. 2012). Hydrogen sulfide derived from AOM in seep systems has also been deemed to facilitate the formation of carbonate minerals with high Mg content, especially dolomite (Lu et al. 2015; Tong et al. 2019). The observed different trends of $\delta^{13}C$ and $\delta^{26}Mg$ values refer to opposite trends in the degree of Mg isotope fractionation with enhanced intensity of AOM (Fig. 10.5). The dissolved H_2S may affect the Mg isotopic composition of carbonates, although the mechanism is still not well

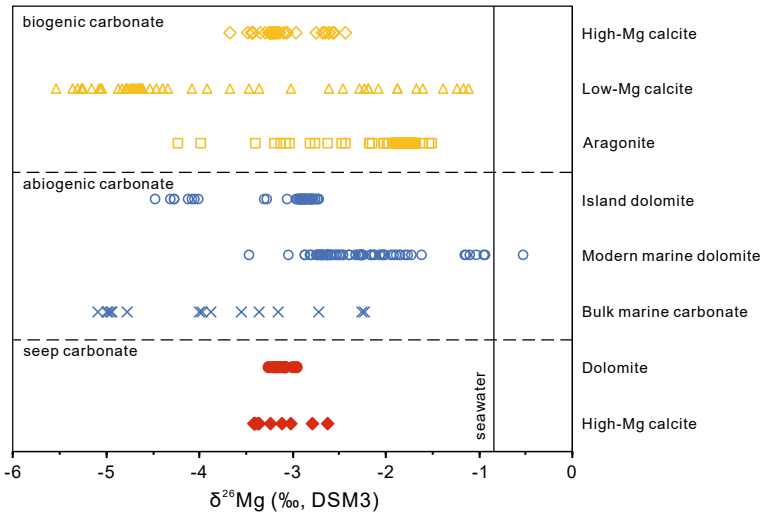

Fig. 10.4 Comparison of magnesium isotopic compositions of carbonates. Data on abiogenic carbonate are from Saenger and Wang (2014) and references therein. Data on island dolomites are from Hu et al. (2022). Data on modern marine dolomites are from Higgins and Schrag (2010), Fantle and Higgins (2014), Mavromatis et al. (2014) and Blättler et al. (2015). Data on dolomite and HMC in seep carbonate are from Lu et al. (2017) and Jin et al. (2021), respectively

understood. This may provide new insights into the application of carbonate Mg isotopic compositions during geological time of widespread oceanic anoxia.

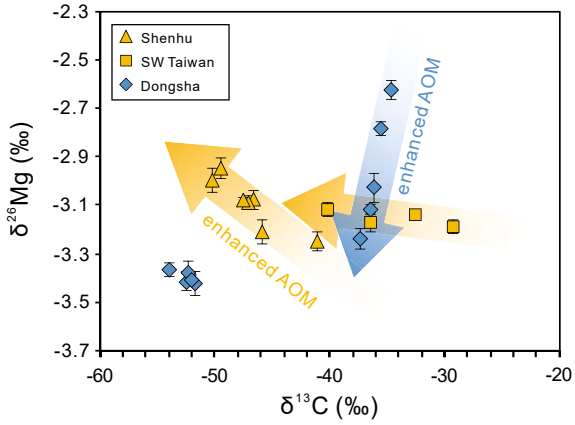

Fig. 10.5 Correlation of inorganic $\delta^{13}C$ and $\delta^{26}Mg$ values of seep carbonates from the South China Sea (modified after Jin et al. 2021). Data from the Shenhu and SW Taiwan areas are from Lu et al. (2017). Data from the Dongsha area are from Jin et al. (2021)

10.5 Ca Isotopes

Calcium is abundant in both terrestrial and marine systems. It has five stable isotopes (^{40}Ca, ^{42}Ca, ^{43}Ca, ^{44}Ca and ^{46}Ca) and a radioactive isotope (^{48}Ca) with an extremely long half-life of 1.9×10^{19} years (Griffith and Fantle 2021). The abundance of isotopes from ^{40} to ^{48}Ca is 96.941%, 0.647%, 0.135%, 2.086%, 0.004% and 0.187%, respectively (Meija et al. 2016). The Ca isotope ratios are expressed as δ^{44}Ca:

$$\delta^{44}\mathrm{Ca} = \left[\frac{\left(^{44}\mathrm{Ca}/^{40}\mathrm{Ca}\right)_{\mathrm{sample}}}{\left(^{44}\mathrm{Ca}/^{40}\mathrm{Ca}\right)_{\mathrm{standard}}} - 1 \right] \times 1000$$

Multiple standards are in use to define δ^{44}Ca, such as SRM 915a, SRM 915b, seawater, and bulk silicate Earth (Griffith and Fantle 2021). Data are reported relative to seawater in the following text. The conversion of δ^{44}Ca relative to SRM 915a and seawater is according to Hippler et al. (2003):

$$\delta^{44}\mathrm{Ca}_{\mathrm{SRM915a}} = \delta^{44}\mathrm{Ca}_{\mathrm{seawater}} + 1.88‰$$

The formation of carbonate plays an important role in the cycling of Ca. The calcium isotopic composition of carbonate has been used to quantify rates of carbonate diagenesis and trace global Ca cycling (Griffith and Fantle 2021). The δ^{44}Ca values of modern marine carbonates generally display isotope fractionations between − 1.8‰ and − 0.8‰ from seawater (Blättler et al. 2012; Fantle and Tipper 2014). Similar to Mg isotopes, carbonate mineralogy and precipitation rate are two dominant factors controlling the calcium isotopic compositions of carbonate (Gussone et al. 2005; Tang et al. 2008; Blättler et al. 2012). The high alkalinity of pore water in seep systems facilitates the formation of authigenic carbonate with a fast precipitation rate (Aloisi et al. 2000; Naehr et al. 2007). The calcium isotopic compositions of seep carbonate may have the potential for understanding the formation process of carbonate during early diagenesis. The diffusion of seawater-dissolved Ca^{2+} into pore water is the main source of authigenic carbonate at seeps. Carbonate depleted in ^{44}Ca indicates that the precipitation of seep carbonate prefers light Ca isotopes (Fig. 10.6). Mg-calcite in seep carbonate yields higher δ^{44}Ca values than aragonite (Fig. 10.6). The reported δ^{44}Ca values of dolomite-dominated seep carbonate from the South China Sea (−0.67‰ to − 0.41‰, n = 11) are similar to those of Mg-calcite (Wang et al. 2012, 2013; Thiagarajan et al. 2020; Blättler et al. 2021). Wang et al. (2012) suggested that the variation in δ^{44}Ca values can be attribute to supersaturation, precipitation rate and the degree of Ca consumption in semi-closed systems at seeps. The Rayleigh effect on Ca isotope fractionation during the precipitation of seep carbonate can also be indicated by the downward-increasing δ^{44}Ca values of pore water from the Storfjordrenna Trough in Blättler et al. (2021).

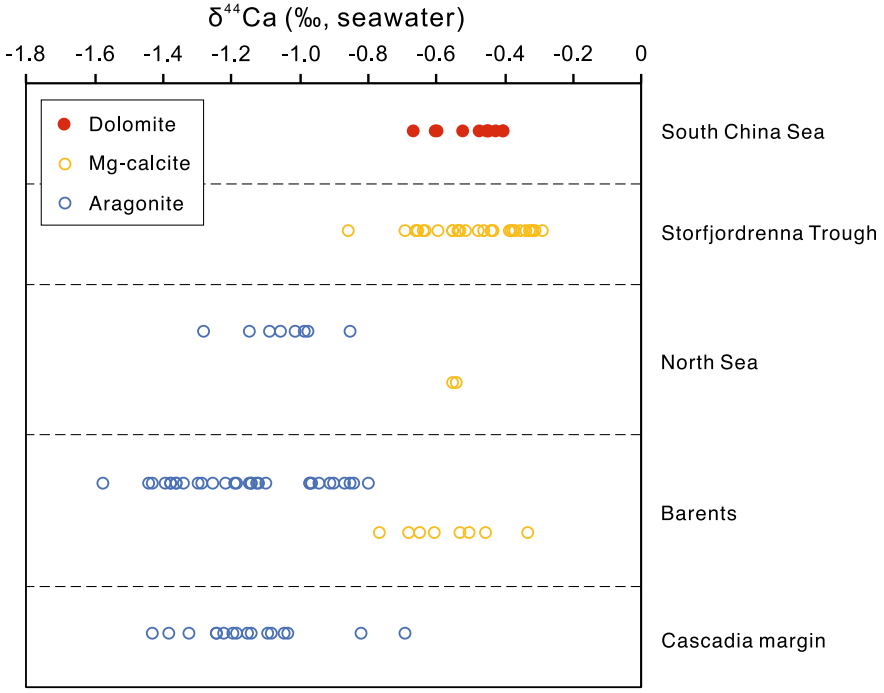

Fig. 10.6 Comparison of Ca isotopic compositions of seep carbonate. Data from the South China Sea are from Wang et al. (2012, 2013). Data from the Storfjordrenna Trough and the North Sea are from Thiagarajan et al. (2020). Data from the Cascadia margin are from Teichert et al. (2005)

10.6 Summary and Future Studies

In summary, the special and complex sedimentary environments in seep systems could impact the behaviors of isotopes, such as Fe, Mo, Mg and Ca. The iron isotopic compositions of pyrite are strongly related to its formation process and ambient environmental conditions. Isotopic signatures of Mo in seep carbonates and sediments are relevant to Mo migration and transformation with a changing redox state. Magnesium and Ca isotopic compositions of seep carbonate reflect the precipitation of authigenic carbonate, and the hydrogen sulfide derived from AOM may significantly influence the fractionation of Mg isotopes. Non-traditional isotope geochemistry in seep systems is still in its infancy. Whether the special environment at seeps affects the fractionation mechanism of these isotopes is unclear. The application potential of these non-traditional isotopic compositions of seep deposits also remains to be developed. Below are some problems in the field of non-traditional isotope geochemistry in seep systems that could be further studied in the future:

1. Pyrite in seep systems is the result of continuous accumulation along with the dynamic activity of methane seepage. The Fe isotopic compositions of pyrite

may be an assemblage of complex biogeochemical processes, especially when multiple seepage events occur. More research is needed to further reveal the information hidden in the Fe isotopic compositions of pyrite.

2. Molybdenum in seep deposits exists in carbonate minerals, sulfide phases, detritus and organic materials. The Mo isotopic signature of bulk seep carbonate is a mixture of the δ^{98}Mo of all these Mo-bearing phases. This causes uncertainty in the application of seep carbonates to trace the Mo isotopic compositions of seawater. Analyzing the Mo isotopic compositions of different phases in seep carbonates by sequential chemical extraction may help to better understand the behavior of Mo isotopes in seep systems.
3. Dissolved hydrogen sulfide plays an important role in the behavior of Mg. Therefore, the AOM in seep systems has been thought to have a possible effect on the fractionation of Mg isotopes during the formation of seep carbonates. The behavior of Mg isotopes during carbonate precipitation under sulfidic conditions could be better constrained by precipitation experiments.
4. Seep carbonates form under a fast precipitation rate. The precipitation rate is an important factor controlling the fractionation of Ca isotopes during carbonate precipitation. However, the Rayleigh effect also obviously influences the δ^{44}Ca of seep carbonates. Therefore, more research is needed to better constrain the precipitation rate of seep carbonate to quantify the effect of the precipitation rate on its Ca isotopic composition.

Acknowledgements The authors are grateful to Yu Hu (Shanghai Ocean University) and Zhiyong Lin (Universität Hamburg) for the constructive comments.

References

Aloisi G, Pierre C, Rouchy JM et al (2000) Methane-related authigenic carbonates of eastern Mediterranean Sea mud volcanoes and their possible relation to gas hydrate destabilisation. Earth Planet Sci Lett 184(1):321–338

Barling J, Arnold GL, Anbar AD (2001) Natural mass-dependent variations in the isotopic composition of molybdenum. Earth Planet Sci Lett 193(3–4):447–457

Beard BL, Johnson CM (1999) High precision iron isotope measurements of terrestrial and lunar materials. Geochim Cosmochim Acta 63(11–12):1653–1660

Beard BL, Johnson CM, Skulan JL et al (2003a) Application of Fe isotopes to tracing the geochemical and biological cycling of Fe. Chem Geol 195(1–4):87–117

Beard BL, Johnson CM, Von Damm KL et al (2003b) Iron isotope constraints on Fe cycling and mass balance in oxygenated Earth oceans. Geology 31(7):629–632

Bekker A, Holland HD, Wang PL et al (2004) Dating the rise of atmospheric oxygen. Nature 427(6970):117–120

Berner RA (1970) Sedimentary pyrite formation. Am J Sci 268:1–23

Blättler CL, Henderson GM, Jenkyns HC (2012) Explaining the Phanerozoic Ca isotope history of seawater. Geology 40(9):843–846

Blättler CL, Hong W-L, Kirsimäe K et al (2021) Small calcium isotope fractionation at slow precipitation rates in methane seep authigenic carbonates. Geochim Cosmochim Acta 298:227–239

Blättler CL, Miller NR, Higgins JA (2015) Mg and Ca isotope signatures of authigenic dolomite in siliceous deep-sea sediments. Earth Planet Sci Lett 419:32–42

Borowski WS, Rodriguez NM, Paull CK et al (2013) Are ^{34}S-enriched authigenic sulfide minerals a proxy for elevated methane flux and gas hydrates in the geologic record? Mar Pet Geol 43:381–395

Butler IB, Archer C, Vance D et al (2005) Fe isotope fractionation on FeS formation in ambient aqueous solution. Earth Planet Sci Lett 236(1–2):430–442

Canfield DE, Teske A (1996) Late Proterozoic rise in atmospheric oxygen concentration inferred from phylogenetic and sulphur-isotope studies. Nature 382(6587):127–132

Chen F, Hu Y, Feng D et al (2016) Evidence of intense methane seepages from molybdenum enrichments in gas hydrate-bearing sediments of the northern South China Sea. Chem Geol 443:173–181

Dauphas N, John SG, Rouxel O (2017) Iron Isotope Systematics. Rev Mineral Geochem 82:415–510

Egger M, Rasigraf O, Sapart CJ et al (2015) Iron-Mediated Anaerobic Oxidation of Methane in Brackish Coastal Sediments. Environ Sci Technol 49(1):277–283

Erickson BE, Helz GR (2000) Molybdenum (VI) speciation in sulfidic waters: Stability and lability of thiomolybdates. Geochim Cosmochim Acta 64(7):1149–1158

Fantle MS, Higgins J (2014) The effects of diagenesis and dolomitization on Ca and Mg isotopes in marine platform carbonates: Implications for the geochemical cycles of Ca and Mg. Geochim Cosmochim Acta 142:458–481

Fantle MS, Tipper ET (2014) Calcium isotopes in the global biogeochemical Ca cycle: Implications for development of a Ca isotope proxy. Earth-Sci Rev 129:148–177

Farquhar J, Bao H, Thiemens M (2000) Atmospheric Influence of Earth's Earliest Sulfur Cycle. Science 289(5480):756–758

Fehr MA, Andersson PS, Hålenius U et al (2010) Iron enrichments and Fe isotopic compositions of surface sediments from the Gotland Deep, Baltic Sea. Chem Geol 277(3–4):310–322

Fehr MA, Andersson PS, Hålenius U et al (2008) Iron isotope variations in Holocene sediments of the Gotland Deep, Baltic Sea. Geochim Cosmochim Acta 72(3): 807–826

Feng D, Qiu J-W, Hu Y et al (2018) Cold seep systems in the South China Sea: An overview. J Asian Earth Sci 168:3–16

Gieskes J, Mahn C, Day S et al (2005) A study of the chemistry of pore fluids and authigenic carbonates in methane seep environments: Kodiak Trench, Hydrate Ridge, Monterey Bay, and Eel River Basin. Chem Geol 220(3–4):329–345

Gieskes J, Rathburn AE, Martin JB et al (2011) Cold seeps in Monterey Bay, California: Geochemistry of pore waters and relationship to benthic foraminiferal calcite. Appl Geochem 26(5):738–746

Griffith EM, Fantle MS (2021) Calcium Isotopes. Cambridge University Press, Cambridge. https://doi.org/10.1017/9781108853972

Guilbaud R, Butler IB, Ellam RM (2011) Abiotic Pyrite Formation Produces a Large Fe Isotope Fractionation. Science 332(6037):1548–1551

Gussone N, Böhm F, Eisenhauer A et al (2005) Calcium isotope fractionation in calcite and aragonite. Geochim Cosmochim Acta 69(18):4485–4494

Halliday AN, Lee D-C, Christensen JN et al (1995) Recent developments in inductively coupled plasma magnetic sector multiple collector mass spectrometry. Int J Mass Spectrom Ion Process 146:21–33

Han X, Suess E, Huang Y et al (2008) Jiulong methane reef: Microbial mediation of seep carbonates in the South China Sea. Mar Geol 249(3–4):243–256

Helz GR, Bura-Nakić E, Mikac N et al (2011) New model for molybdenum behavior in euxinic waters. Chem Geol 284(3–4):323–332

Helz GR, Miller CV, Charnock JM et al (1996) Mechanism of molybdenum removal from the sea and its concentration in black shales: EXAFS evidence. Geochim Cosmochim Acta 60(19):3631–3642

Higgins JA, Schrag DP (2010) Constraining magnesium cycling in marine sediments using magnesium isotopes. Geochim Cosmochim Acta 74(17):5039–5053

Higgins JA, Schrag DP (2012) Records of Neogene seawater chemistry and diagenesis in deep-sea carbonate sediments and pore fluids. Earth Planet Sci Lett 357:386–396

Higgins JA, Schrag DP (2015) The Mg isotopic composition of Cenozoic seawater – evidence for a link between Mg-clays, seawater Mg/Ca, and climate. Earth Planet Sci Lett 416:73–81

Hippler D, Schmitt A-D, Gussone N et al (2003) Calcium Isotopic Composition of Various Reference Materials and Seawater. Geostand Newsl 27(1):13–19

Hlohowskyj SR, Chappaz A, Dickson AJ (2021) Molybdenum as a Paleoredox Proxy: Past, Present, and Future. Cambridge University Press, Cambridge. https://doi.org/10.1017/9781108993777

Hofmann A, Bekker A, Rouxel O et al (2009) Multiple sulphur and iron isotope composition of detrital pyrite in Archaean sedimentary rocks: A new tool for provenance analysis. Earth Planet Sci Lett 286(3–4):436–445

Hu Y, Feng D, Liang Q et al (2015) Impact of anaerobic oxidation of methane on the geochemical cycle of redox-sensitive elements at cold-seep sites of the northern South China Sea. Deep-Sea Res Part II-Top Stud Oceanogr 122:84–94

Hu Y, Feng D, Peckmann J et al (2014) New insights into cerium anomalies and mechanisms of trace metal enrichment in authigenic carbonate from hydrocarbon seeps. Chem Geol 381:55–66

Hu Z, Shi Z, Li G et al (2022) The Cenozoic Seawater Conundrum: New constraints from Mg isotopes in island dolostones. Earth Planet Sci Lett 595:117755

Jin M, Feng D, Huang K et al (2022) Magnesium Isotopes in Pore Water of Active Methane Seeps of the South China Sea. Front Mar Sci 9:858860

Jin M, Feng D, Huang K et al (2021) Behavior of Mg isotopes during precipitation of methane-derived carbonate: Evidence from tubular seep carbonates from the South China Sea. Chem Geol 567:120101

Johnson CM, Beard BL, Roden EE (2008) The Iron Isotope Fingerprints of Redox and Biogeochemical Cycling in Modern and Ancient Earth. Annu Rev Earth Planet Sci 36:457–493

Johnson CM, Skulan JL, Beard BL et al (2002) Isotopic fractionation between Fe(III) and Fe(II) in aqueous solutions. Earth Planet Sci Lett 195(1–2):141–153

Johnston DT, Poulton SW, Fralick PW et al (2006) Evolution of the oceanic sulfur cycle at the end of the Paleoproterozoic. Geochim Cosmochim Acta 70(23):5723–5739

Jørgensen BB, Böttcher ME, Lüschen H et al (2004) Anaerobic methane oxidation and a deep H_2S sink generate isotopically heavy sulfides in Black Sea sediments. Geochim Cosmochim Acta 68:2095–2118

Jørgensen BB, Kasten S (2006) Sulfur Cycling and Methane Oxidation. In: Schulz HD, Zabel M (eds) Marine Geochemistry. Springer, Berlin Heidelberg, Berlin, Heidelberg, pp 271–309

Joye SB, Bowles MW, Samarkin VA et al (2010) Biogeochemical signatures and microbial activity of different cold-seep habitats along the Gulf of Mexico deep slope. Deep-Sea Res Part II-Top Stud Oceanogr 57(21–23):1990–2001

Kendall B, Dahl TW, Anbar AD (2017) The Stable Isotope Geochemistry of Molybdenum. Rev Mineral Geochem 82:683–732

Li Y-H (1982) A brief discussion on the mean oceanic residence time of elements. Geochim Cosmochim Acta 46(12):2671–2675

Lin Z, Sun X, Chen K et al (2022) Effects of sulfate reduction processes on the trace element geochemistry of sedimentary pyrite in modern seep environments. Geochim Cosmochim Acta 333:75–94

Lin Z, Sun X, Lu Y et al (2018) Iron isotope constraints on diagenetic iron cycling in the Taixinan seepage area, South China Sea. J Asian Earth Sci 168:112–124

Lin Z, Sun X, Peckmann J et al (2016) How sulfate-driven anaerobic oxidation of methane affects the sulfur isotopic composition of pyrite: A SIMS study from the South China Sea. Chem Geol 440:26–41

Lin Z, Sun X, Lu Y et al (2017) The enrichment of heavy iron isotopes in authigenic pyrite as a possible indicator of sulfate-driven anaerobic oxidation of methane: Insights from the South China Sea. Chem Geol 449:15–29

Lin Z, Sun X, Strauss H et al (2021) Molybdenum isotope composition of seep carbonates – Constraints on sediment biogeochemistry in seepage environments. Geochim Cosmochim Acta 307:56–71

Ling M-X, Sedaghatpour F, Teng F-Z et al (2011) Homogeneous magnesium isotopic composition of seawater: an excellent geostandard for Mg isotope analysis. Rapid Commun Mass Spectrom 25(19):2828–2836

Liu J, Pellerin A, Antler G et al (2020) Early diagenesis of iron and sulfur in Bornholm Basin sediments: The role of near-surface pyrite formation. Geochim Cosmochim Acta 284:43–60

Lu Y, Liu Y, Sun X et al (2017) Intensity of methane seepage reflected by relative enrichment of heavy magnesium isotopes in authigenic carbonates: A case study from the South China Sea. Deep-Sea Res Part I-Oceanogr Res Pap 129:10–21

Lu Y, Sun XM, Lin ZY et al (2015) Cold seep status archived in authigenic carbonates: Mineralogical and isotopic evidence from Northern South China Sea. Deep-Sea Res Part II-Top Stud Oceanogr 122:95–105

Lu Y, Sun XM, Xu HF et al (2018) Formation of dolomite catalyzed by sulfate-driven anaerobic oxidation of methane: Mineralogical and geochemical evidence from the northern South China Sea. Am Miner 103(5):720–734

Lu Y, Yang X, Lin Z et al (2021) Reducing microenvironments promote incorporation of magnesium ions into authigenic carbonate forming at methane seeps: Constraints for dolomite formation. Sedimentology 68(7):2945–2964

Mavromatis V, Immenhauser A, Buhl D et al (2017) Effect of organic ligands on Mg partitioning and Mg isotope fractionation during low-temperature precipitation of calcite in the absence of growth rate effects. Geochim Cosmochim Acta 207:139–153

Mavromatis V, Meister P, Oelkers EH (2014) Using stable Mg isotopes to distinguish dolomite formation mechanisms: A case study from the Peru Margin. Chem Geol 385:84–91

Meija J, Coplen TB, Berglund M et al (2016) Isotopic compositions of the elements 2013 (IUPAC Technical Report). Pure Appl Chem 88(3):293–306

Miller CA, Peucker-Ehrenbrink B, Walker BD et al (2011) Re-assessing the surface cycling of molybdenum and rhenium. Geochim Cosmochim Acta 75(22):7146–7179

Naehr TH, Eichhubl P, Orphan VJ et al (2007) Authigenic carbonate formation at hydrocarbon seeps in continental margin sediments: A comparative study. Deep-Sea Res Part II-Top Stud Oceanogr 54(11–13):1268–1291

Nägler TF, Anbar AD, Archer C et al (2014) Proposal for an International Molybdenum Isotope Measurement Standard and Data Representation. Geostand Geoanal Res 38(2):149–151

Nägler TF, Neubert N, Böttcher ME et al (2011) Molybdenum isotope fractionation in pelagic euxinia: Evidence from the modern Black and Baltic Seas. Chem Geol 289(1–2):1–11

Nakagawa Y, Takano S, Firdaus ML et al (2012) The molybdenum isotopic composition of the modern ocean. Geochem J 46(2):131–141

Neubert N, Nägler TF, Böttcher ME (2008) Sulfidity controls molybdenum isotope fractionation into euxinic sediments: Evidence from the modern Black Sea. Geology 36(10):775–778

Pasquier V, Sansjofre P, Rabineau M et al (2017) Pyrite sulfur isotopes reveal glacial−interglacial environmental changes. Proc Natl Acad Sci U S A 114(23):5941–5945

Peckmann J, Reimer A, Luth U et al (2001) Methane-derived carbonates and authigenic pyrite from the northwestern Black Sea. Mar Geol 177(1–2):129–150

Poulson RL, Siebert C, McManus J et al (2006) Authigenic molybdenum isotope signatures in marine sediments. Geology 34(8):617–620

Poulton SW, Krom MD, Raiswell R (2004) A revised scheme for the reactivity of iron (oxyhydr)oxide minerals towards dissolved sulfide. Geochim Cosmochim Acta 68(18):3703–3715

Riedinger N, Formolo MJ, Lyons TW et al (2014) An inorganic geochemical argument for coupled anaerobic oxidation of methane and iron reduction in marine sediments. Geobiology 12(2):172–181

Rouxel OJ, Bekker A, Edwards KJ (2005) Iron Isotope Constraints on the Archean and Paleoproterozoic Ocean Redox State. Science 307:1088–1091

Saenger C, Wang ZR (2014) Magnesium isotope fractionation in biogenic and abiogenic carbonates: implications for paleoenvironmental proxies. Quat Sci Rev 90:1–21

Scholz F, Severmann S, McManus J et al (2014) On the isotope composition of reactive iron in marine sediments: Redox shuttle versus early diagenesis. Chem Geol 389:48–59

Scholz F, Siebert C, Dale AW et al (2017) Intense molybdenum accumulation in sediments underneath a nitrogenous water column and implications for the reconstruction of paleo-redox conditions based on molybdenum isotopes. Geochim Cosmochim Acta 213:400–417

Schott J, Mavromatis V, Fujii T et al (2016) The control of carbonate mineral Mg isotope composition by aqueous speciation: Theoretical and experimental modeling. Chem Geol 445:120–134

Scott C, Lyons TW (2012) Contrasting molybdenum cycling and isotopic properties in euxinic versus non-euxinic sediments and sedimentary rocks: Refining the paleoproxies. Chem Geol 324:19–27

Severmann S, Johnson CM, Beard BL et al (2006) The effect of early diagenesis on the Fe isotope compositions of porewaters and authigenic minerals in continental margin sediments. Geochim Cosmochim Acta 70(8):2006–2022

Siebert C, Nägler TF, von Blanckenburg F et al (2003) Molybdenum isotope records as a potential new proxy for paleoceanography. Earth Planet Sci Lett 211(1–2):159–171

Tang J, Dietzel M, Böhm F et al (2008) Sr^{2+}/Ca^{2+} and $^{44}Ca/^{40}Ca$ fractionation during inorganic calcite formation: II. Ca Isotopes. Geochim Cosmochim Acta 72(15):3733–3745

Teichert BMA, Gussone N, Eisenhauer A et al (2005) Clathrites: Archives of near-seafloor pore-fluid evolution ($\delta^{44}/^{40}Ca$, $\delta^{13}C$, $\delta^{18}O$) in gas hydrate environments. Geology 33(3):213–216

Teng F-Z (2017) Magnesium Isotope Geochemistry. Rev Mineral Geochem 82:219–287

Teng F-Z, Dauphas N, Watkins JM (2017) Non-Traditional Stable Isotopes: Retrospective and Prospective. Rev Mineral Geochem 82:1–26

Thiagarajan N, Crémière A, Blättler C et al (2020) Stable and clumped isotope characterization of authigenic carbonates in methane cold seep environments. Geochim Cosmochim Acta 279:204–219

Tipper E, Galy A, Gaillardet J et al (2006) The magnesium isotope budget of the modern ocean: Constraints from riverine magnesium isotope ratios. Earth Planet Sci Lett 250(1–2):241–253

Tong H, Feng D, Peckmann J et al (2019) Environments favoring dolomite formation at cold seeps: A case study from the Gulf of Mexico. Chem Geol 518:9–18

Tribovillard N, Algeo TJ, Lyons T et al (2006) Trace metals as paleoredox and paleoproductivity proxies: An update. Chem Geol 232(1–2):12–32

Wang S, Yan W, Magalhães HV et al (2012) Calcium isotope fractionation and its controlling factors over authigenic carbonates in the cold seeps of the northern South China Sea. Chin Sci Bull 57(11):1325–1332

Wang S, Yan W, Magalhães VH et al (2013) Factors influencing methane-derived authigenic carbonate formation at cold seep from southwestern Dongsha area in the northern South China Sea. Environ Earth Sci 71(5):2087–2094

Wasylenki LE, Rolfe BA, Weeks CL et al (2008) Experimental investigation of the effects of temperature and ionic strength on Mo isotope fractionation during adsorption to manganese oxides. Geochim Cosmochim Acta 72(24):5997–6005

Welch SA, Beard BL, Johnson CM et al (2003) Kinetic and equilibrium Fe isotope fractionation between aqueous Fe (II) and Fe (III). Geochim Cosmochim Acta 67(22):4231–4250

Wu L, Druschel G, Findlay A et al (2012) Experimental determination of iron isotope fractionations among Fe_{aq}^{2+}–FeS_{aq}–Mackinawite at low temperatures: Implications for the rock record. Geochim Cosmochim Acta 89:46–61

Young ED, Galy A (2004) The Isotope Geochemistry and Cosmochemistry of Magnesium. Rev Mineral Geochem 55:197–230

Zhang FF, Xu HF, Konishi H et al (2012) Dissolved sulfide-catalyzed precipitation of disordered dolomite: Implications for the formation mechanism of sedimentary dolomite. Geochim Cosmochim Acta 97:148–165